

# Linear plasmon dispersion in single-wall carbon nanotubes and the collective excitation spectrum of graphene

C. Kramberger,<sup>1</sup> R. Hambach,<sup>2,3</sup> C. Giorgetti,<sup>2</sup> M. H. Rummeli,<sup>1</sup> M. Knupfer,<sup>1</sup> J. Fink,<sup>1,4</sup> B. Büchner,<sup>1</sup> L. Reining,<sup>2</sup> E. Einarsson,<sup>5</sup> S. Maruyama,<sup>5</sup> F. Sottile,<sup>2</sup> K. Hannewald,<sup>3</sup> V. Olevano,<sup>6</sup> A.G. Marinopoulos,<sup>7,8</sup> and T. Pichler<sup>1,9</sup>

<sup>1</sup>*IFW Dresden, Helmholtzstr. 20, D-01069 Dresden, Germany*

<sup>2</sup>*Laboratoire des Solides Irradiés, CEA-CNRS UMR 7642-Ecole Polytechnique, 91128 Palaiseau Cedex, France and European Theoretical Spectroscopy Facility (ETSF), Palaiseau, France*

<sup>3</sup>*IFTO, Friedrich-Schiller-Universität Jena, 07743 Jena, Germany*

<sup>4</sup>*BESSY II, D-12489 Berlin, Germany*

<sup>5</sup>*The Univ. of Tokyo, Dept. of Mech. Eng., 7-3-1 Hongo, Bunkyo-ku, Tokyo 113-8656, Japan*

<sup>6</sup>*Institut Néel, Grenoble, France and European Theoretical Spectroscopy Facility (ETSF), Palaiseau, France*

<sup>7</sup>*Laboratoire des Solides Irradiés, CEA-CNRS UMR 7642-Ecole Polytechnique, 91128 Palaiseau Cedex, France*

<sup>8</sup>*Department of Physics and Astronomy, Vanderbilt University, Nashville, TN 37235, USA*

<sup>9</sup>*Institute of Materials Physics, University of Vienna, Strudlhofgasse 4, A-1090, Vienna, Austria*

(Dated: submitted to Phys. Rev. Lett., February 1, 2008)

We have measured a strictly linear  $\pi$  plasmon dispersion along the axis of individualized single wall carbon nanotubes, which is completely different from plasmon dispersions of graphite or bundled single wall carbon nanotubes. Comparative *ab initio* studies on graphene based systems allow us to reproduce the different dispersions. This suggests that individualized nanotubes provide viable experimental access to collective electronic excitations of graphene, and it validates the use of graphene to understand electronic excitations of carbon nanotubes. In particular, the calculations reveal that local field effects (LFE) cause a mixing of electronic transitions, including the ‘Dirac cone’, resulting in the observed linear dispersion.

PACS numbers: 73.20.Mf, 73.22.-f, 78.20.Bh

Single-wall carbon nanotubes (SWNT) and its parent compound graphene are archetypes of low dimensional systems with strongly anisotropic and unique electronic properties which make them interesting for both fundamental research and as building blocks in nanoelectronic applications [1]. Their electronic bandstructure is frequently studied. In graphene, the linear band dispersion at the Fermi level, the ‘Dirac cone’, leads to unique characteristics in nanoelectronic devices [2]. One can expect a strong analogy between graphene and isolated SWNT for excitations along the sheet and along the tube axis, respectively. Within the zone-folding model, i.e. neglecting curvature effects, the graphene bandstructure is sliced along parallel lines when the sheet is rolled up into a cylinder. The result are characteristic van Hove singularities (VHS) in the density of states (DOS) [3]. Bulk (i.e. bundled) SWNT show an optical absorption peak at  $\sim 4.5$  eV due to transitions of the  $\pi$  electrons [4]. In vertically aligned SWNT (VA-SWNT) one finds the same peak position for on-axis polarization and an additional peak for perpendicular polarization at  $\sim 5.2$  eV [5]. Further information can be obtained from collective electronic excitations (plasmons) beyond the optical limit [6] (i.e. momentum transfer  $q > 0$ ). Angle resolved electron energy loss spectroscopy (EELS) assesses the detailed plasmon dispersion [7, 8], but it is so far missing for freestanding isolated  $sp^2$  carbon systems.

Models based on the homogeneous electron gas [9], or the tight-binding scheme [10, 11] have been used to describe these excitations. The former are however bound to metallic systems. The latter have provided valuable insight and predictions for the properties of isolated sheets, tubes, and assemblies of these objects; in particular, they have predicted an

almost linear plasmon dispersion for isolated systems. However, the tight binding results neglect screening beyond the  $\pi$  bands, and they depend on parameters that hide the underlying complexity. No realistic parameter-free calculations have been performed to predict the plasmon dispersion in these systems, nor has its origin been analyzed. Instead, *ab initio* spectroscopy calculations have dealt with absorption spectra ( $q \rightarrow 0$ ) for SWNT [12, 13, 14], and plasmon dispersions in graphite [15, 16]; most other available calculations are *ground-state* or *bandstructure* ones [17]. The prediction, comparison and interpretation of the full dispersive electronic excitations of isolated SWNT and graphene sheets calls for new experiments and for *ab initio* theoretical support going beyond bandstructure calculations.

Indeed, electronic excitations imply a self-consistent response of the entire system and have therefore to be described in terms of bandstructure *and* induced potentials. In solids, the latter consist of microscopic induced components (local field effects [18]) and a macroscopic induced component. The latter is responsible for the difference between interband transitions as measured in absorption, and plasmons as measured in loss spectroscopies [19]. In isolated systems, the macroscopic component will naturally vanish. Absorption peaks and loss peaks at  $q \rightarrow 0$  will hence coincide. The microscopic part, instead, can become dramatically important when macroscopic screening is low. Therefore, theory based on bandstructure alone will be unable to describe isolated systems, whereas experiments performed on bundles or graphite are not representative for isolated SWNT and graphene. There is hence an important gap in our understanding of the properties of these isolated  $sp^2$  carbon systems.

The present work is meant to bridge this gap with a detailed EELS study on freestanding mats of VA-SWNT, and corresponding *ab initio* calculations for graphene sheets. Our studies allow us to give answers to several important questions, by (i) *distinguishing a localized perpendicular and a strictly linear on-axis plasmon dispersion in isolated single-wall nanotubes*; (ii) *showing the quantitative similarity to electronic excitations in graphene*; (iii) *analyzing the impact of local field effects on the linear plasmon dispersion, in particular the mixing-in of low-energy transitions*; (iv) *quantifying the importance of interactions between neighboring sheets or tubes*.

2  $\mu\text{m}$  to 7  $\mu\text{m}$  thick VA-SWNT material was directly grown by catalytic decomposition of alcohol and subsequently detached from the supporting silicon wafers by floating off in hot water and transferred onto Cu grids [20]. The nematic order as well as optical properties [5, 21] and local morphology in transmission electron microscopy of VA-SWNT [22] have been studied earlier. The VA-SWNT are aligned within  $25^\circ$  and typically packed in small bundles with less than 10 nanotubes, each with a diameter of about 2 nm. The angle resolved loss function of the VA-SWNT was measured in a purpose built EELS spectrometer [23]. Earlier comparative EELS studies were performed on a cleaved single crystal [15] of graphite or bundled and magnetically aligned SWNT [8]. In the present study we set an energy and momentum resolution of 200 meV and  $0.05 \text{ \AA}^{-1}$  at a primary incidence energy of 172 keV. Concerning our *ab initio* simulations for isolated single- and double-layer graphene, we start from DFT-LDA ground state calculations [24], using a plane-wave basis set<sup>1</sup> and norm-conserving pseudopotentials of Troullier-Martins type [25]. The loss function is determined within the random phase approximation (RPA) using the DP-code<sup>2</sup>. The local field effects (LFE) that originate from the induced Hartree potential are taken into account, comprising in-plane local fields with spatial variations on the atomic scale (Umklapp effects). Moreover, all contributing valence-electron bands ( $\pi$  and  $\sigma$  as well as empty states) are included. Moving on to our EELS measurements on VA-SWNT, we first inspect the loss function at the lowest momentum transfer ( $0.1 \text{ \AA}^{-1}$ ), depicted topmost in Fig. 1a. We observe peaks corresponding to the  $\pi$  and the more structured  $\pi + \sigma$  plasmon at 5.1 eV and 17.6 eV, respectively. These values are remarkably low for  $\text{sp}^2$  hybridized carbon [8, 26] which indicates minimal macroscopic screening and therefore fits well to the morphological investigations of Einarsson et al. [22]. TEM micrographs in Fig. 1b&c show the cross section and side view of this thin bundled VA-SWNT. For increasing momentum transfer, the loss spectra change significantly (shown up to  $1.0 \text{ \AA}^{-1}$ ). Apparently, both, the  $\pi$  and  $\pi + \sigma$  plasmon split into two distinct contributions; one is localized like in a molecule and another is dispersive like in a solid. We interpret the localized re-

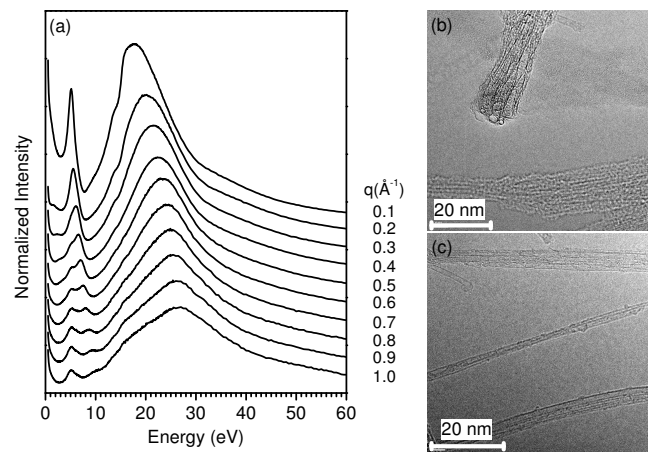


FIG. 1: (a) measured loss function of freestanding VA-SWNT at equidistant  $q$  from  $0.1 \text{ \AA}^{-1}$  (top) to  $1.0 \text{ \AA}^{-1}$  (bottom). And TEM micrographs of the cross section (b) and side view (c) of the thin bundled VA-SWNT

sponse as a contribution with momenta perpendicular to the axis, where an isolated quantum wire becomes a confined dot. The dispersive response belongs to momenta parallel to the nanotube axis, where we encounter an isolated one dimensional wire. The simultaneous, but distinct, observation of these two intrinsic aspects of nanotubes - being *solid-like* at the one hand and *molecule-like* at the other - is a fingerprint of fully individualized viz. ideal wires in terms of plasmon excitations. Following this interpretation, the extrapolation of the corresponding  $\pi$  plasmon position to the optical limit ( $q \rightarrow 0$ ) predicts values of 4.6 eV and 5.1 eV for the on-axis and perpendicular component, respectively (see Fig. 2). This is in excellent agreement with the optical absorption findings of Murakami et al. [5]. Focusing on the dispersive on-axis part of the  $\pi$  plasmon we find a strikingly linear behavior (filled diamonds in Fig. 2d) up to about  $1 \text{ \AA}^{-1}$ , covering more than one third of the Brillouin zone. The linear behavior is totally different from the parabolic  $\pi$  plasmon dispersion of bulk graphite (filled triangles in Fig. 2b), while bulk aligned SWNT (filled circles [8] in Fig. 2c) represent an intermediate situation. Therefore, the plasmon dispersion at low  $q$  is indeed a fingerprint for the degree of isolation. The strictly linear dispersion of the  $\pi$  plasmon is only visible in isolated tubes.

Although this dispersion might resemble the linear dispersion of ‘Dirac electrons’ in graphene, the structures seen in our VA-SWNT measurements (4–9 eV) are clearly outside the energy range of linear band dispersion in graphene. Nevertheless, we will show in the following that graphene *is* indeed *the* system to be used for the interpretation of the on-axis  $\pi$  plasmon dispersion of VA-SWNT. Our *ab initio* calculations allow us to isolate unambiguously the features of this prototype system.

To this aim, the loss function  $-\text{Im} \epsilon^{-1}(\vec{q}, \omega)$  of graphene was calculated for different momentum transfers  $\vec{q}$  along the

<sup>1</sup> We used 3481 k-points and an energy cutoff of 28 Hartree.

<sup>2</sup> <http://www.dp-code.org>; V. Olevano, et al., unpublished.

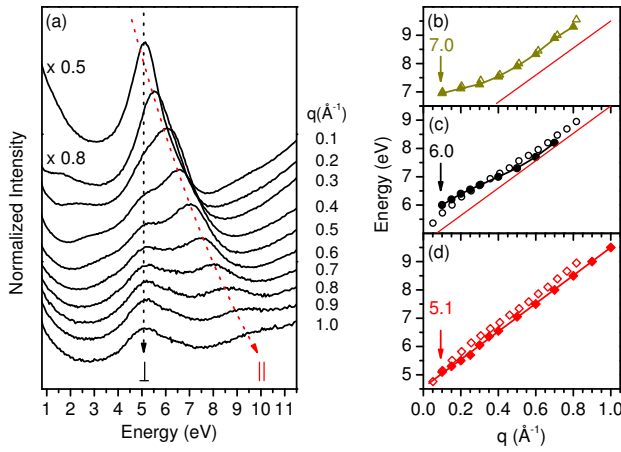


FIG. 2: (color online) (a) loss function of the  $\pi$  plasmon region at equidistant  $q$  ranging from  $0.1 \text{ \AA}^{-1}$  (top) to  $1.0 \text{ \AA}^{-1}$  (bottom). Right stack: observed (filled symbols) vs. calculated (open symbols)  $\pi$  plasmon dispersion for (b) graphite, (c) bundled SWNT [8] vs. double layer graphene and (d) VA-SWNT vs. graphene. The calculations are averaged over the two in-plane directions  $\Gamma K$  and  $\Gamma M$ .

in-plane  $\Gamma M$  and  $\Gamma K$  directions, for values of  $q = |\vec{q}|$  ranging from  $0.05$  to  $0.8 \text{ \AA}^{-1}$ . Starting with the bare RPA (without LFE), the loss function is determined by the independent-particle response function  $\chi_0$ , as in that case  $\text{Im} \epsilon^{-1} \propto \text{Im} \chi_0$ . The resulting spectra can hence be interpreted as a sum of independent transitions, which are directly related to the bandstructure. Fig. 3a shows a typical spectrum for  $q = 0.41 \text{ \AA}^{-1}$ . In the low energy ( $< 10 \text{ eV}$ ) region, only transitions between the  $\pi$  and  $\pi^*$ -band contribute to the spectrum, which consists of three peaks in  $\Gamma M$  direction (thin green line) but only two peaks for  $\Gamma K$  (not shown). In Fig. 3b the corresponding dispersions are depicted (green solid and blue dotted lines, respectively). The first peak arising from transitions within the ‘Dirac cone’ at K starts for the lowest  $q$  at  $0.5 \text{ eV}$  and disperses *linearly* to  $4.0 \text{ eV}$  for the largest  $q$ . The second peak, only visible for  $\Gamma M$  is a weaker structure around  $4 \text{ eV}$  which shows almost no dispersion. The last peak starting at  $4.0 \text{ eV}$  shows a quadratic dispersion at small  $q$ . It can be attributed to transitions near the edge of the Brillouin zone close to M. This peak is almost undetectable in the joint density of states (see dotted curve in Fig. 3a) but is strongly enhanced by matrix elements: already at the independent particle level, bandstructure alone is not sufficient to describe the spectrum completely.

When LFE are included in the calculation one determines  $\epsilon^{-1} = 1 + v\chi$  from the full response function  $\chi = \chi_0 + \chi_0 v \chi$ , where the bare Coulomb interaction  $v$  reflects the variation of the Hartree potential. The inclusion of this term accounts for LFE and changes the results drastically (thick red lines): whereas induced microscopic components have only little effect on the in-plane excitations in bulk graphite [16], LFE are of major importance for the isolated sheets. Most importantly, they completely suppress the linearly dispersing low energy structure as well as the very weakly dispersing second peak.

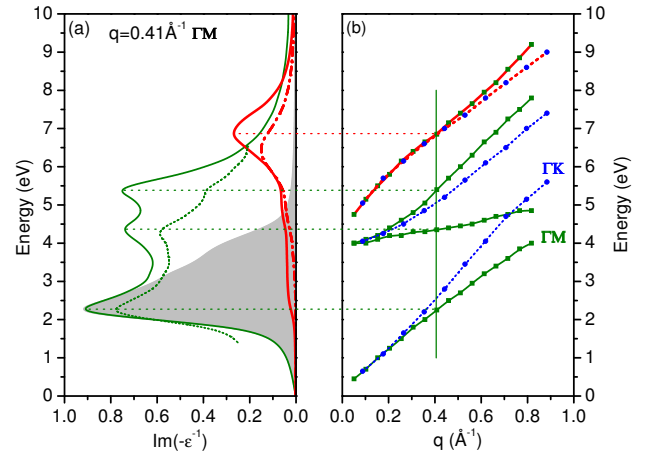


FIG. 3: (color online) (a) loss function of graphene at  $q = 0.41 \text{ \AA}^{-1}$  along  $\Gamma M$  calculated from the JDOS (green dots), within the bare RPA (green) and in RPA including LFE (red, thick). The latter changes significantly, when transitions next to the K point (shaded area), are excluded (red, dot-dashed). (b) dispersion of the peaks in the loss function for different momenta along  $\Gamma M$  (solid lines & squares) and  $\Gamma K$  (dotted lines & circles)

Instead, the peak starting at  $4 \text{ eV}$  is blue shifted by about  $0.8 \text{ eV}$  and becomes the dominant structure in the spectrum. Its dispersion is strongly modified: LFE transform the formerly quadratic dispersion into an almost linear one (red line in Fig. 3b). One can understand the LFE as a mixing of transitions that occurs in the inversions when one solves the screening equation for  $\chi = (\chi_0^{-1} - v)^{-1}$ . Therefore, the resulting spectra should consist of mixtures of the formally distinct peaks. This can involve a significant energy range. It is therefore most interesting, to analyze whether the linearly dispersing low energy peak has considerable influence on the spectra including LFE. By choosing which transitions we include in  $\chi_0$ , we compare the spectra with and without the contributions from the linear region of the  $\pi$ -bands around the K point (i. e. low energy transitions). In the bare RPA loss function  $\chi_0$  this region gives rise to the shaded low energy peak in Fig. 3a. Despite the very different energy ranges, the final loss function after inclusion of LFE is indeed significantly affected by the inclusion (red solid line) or exclusion (red dot-dashed line) of these transitions: in the latter case the dominant structure is strongly reduced (the integrated intensity decreases by more than 30%) and is red shifted by about  $0.4 \text{ eV}$ . There are, hence, considerable contributions from low energy transitions in the LFE corrected plasmon response. With the mixing of transitions of different energies also the different dispersion relations mix; therefore, the resulting almost linear dispersion is indeed a superposition of the dispersion of the main structures in the spectrum, including that resulting from the ‘Dirac cone’.

Figure 2d shows the resulting almost linearly dispersing  $\pi$  plasmon of graphene (open diamonds) together with the on-axis  $\pi$  plasmon of VA-SWNT (filled diamonds). The

graphene plasmon reproduces qualitatively, and even quantitatively, the experimental findings on individualized VA-SWNT. Since our results are completely parameter free, we can conclude that beyond qualitative arguments concerning the tight relation of bandstructures and a similar mechanism of the LFE, graphene can be studied in order to get insight and quantitative information about VA-SWNT, and vice versa.

We now move on to elucidate the interacting case of bundled tubes as shown in Fig. 2c. Experiments on bulk SWNT (filled circles [8]) revealed an asymptotic dispersion relation: the  $\pi$  plasmon is initially shifted to higher energies at small  $q$  before it approaches the linear dispersion of VA-SWNT at large  $q \gtrsim 0.5 \text{ \AA}^{-1}$ . We employ bilayer graphene as an appropriate model system for representing a typical next neighbor situation. Indeed, the calculated  $\pi$  plasmon dispersion of isolated double layer graphene with an interlayer distance of  $d = 3.3 \text{ \AA}$  (as in graphite) shows the same overall behavior (open circles) as the measurements on bundled tubes: we find a transition from a regime, where the Coulomb interaction  $v \propto q^{-2}$  yields long range contributions involving neighboring layers, to a situation where  $q$  is sufficiently large to confine main interactions to the same plane. In particular, we studied at which interlayer distance  $d$  the crossover from interacting to non-interacting sheets occurs. For small  $q = 0.1 \text{ \AA}^{-1}$ , a distance of  $30 \text{ \AA}$  is necessary in order to suppress the influence of neighboring sheets on the spectra, while for  $q = 1.3 \text{ \AA}^{-1}$  the interlayer distance can be reduced to  $7 \text{ \AA}$ . In close analogy, the distinct  $\pi$  plasmon dispersion of bundled SWNT represents a smooth dimensional crossover from three dimensional bundles to one dimensional separated wires. Hence high  $q$  measurements are applicable to probe the intrinsic properties of individual tubes in bundles.

Summarizing, we observe distinct  $\pi$  plasmon dispersions in bulk graphite, bundled SWNT and individualized VA-SWNT. Owing to the individualization in the VA-SWNT we find a localized perpendicular and a strictly linear on-axis  $\pi$  plasmon dispersion. Our *ab initio* studies uncover drastic changes of the spectral RPA response of graphene upon the inclusion of local field effects. These LFE account for a linearly dispersing  $\pi$  plasmon in isolated graphene. If a system can be considered to be isolated or not depends strongly upon the momentum transfer  $q$ . In bundled SWNT a transition from an interacting to a quasi non-interacting regime for large  $q$  occurs and leads to an asymptotic dispersion relation. Measurements on VA-SWNT assisted by calculations on graphene-based systems can hence discern the contributions of the building blocks and their interaction, and show that the study of a prototype system of this kind can be used to obtain insight into the collective electronic excitations of related materials.

**Acknowledgements:** This work was supported by the DFG PI 440 3/4, the EU's 6th Framework Programme through the NANOQUANTA Network of Excellence (NMP4-CT-2004-500198) and by the ANR (project NT0S-3 43900). Computer time was provided by IDRIS (project 544). C. K. acknowledges the *IMPRS for Dynamical Processes in Atoms,*

*Molecules and Solids.* R. H. thanks the Dr. Carl Duisberg-Stiftung and C'Nano IdF (IF07-800/R). We thank S. Leger, R. Hübel, and R. Schönfelder for technical assistance.

- 
- [1] P. Avouris and J. Chen, *Materials Today* **9**, 46 (2006).
  - [2] A. K. Geim and K. S. Novoselov, *Nature Materials* **6**, 183 (2007).
  - [3] N. Hamada, S. I. Sawada, and A. Oshiyama, *Phys. Rev. Lett.* **68**, 1579 (1992).
  - [4] H. Kataura, Y. Kumazawa, Y. Maniwa, I. Umezumi, S. Suzuki, Y. Ohtsuka, and Y. Achiba, *Synth. Met.* **103**, 2555 (1999).
  - [5] Y. Murakami, E. Einarsson, T. Edamura, and S. Maruyama, *Phys. Rev. Lett.* **94**, 087402 (2005).
  - [6] O. Stephan, D. Taverna, M. Kociak, K. Suenaga, L. Henrard, and C. Colliex, *Phys. Rev. B* **66**, 155422 (2002).
  - [7] T. Pichler, M. Knupfer, M. S. Golden, J. Fink, A. Rinzler, and R. E. Smalley, *Phys. Rev. Lett.* **80**, 4729 (1998).
  - [8] X. Liu, T. Pichler, M. Knupfer, M. S. Golden, J. Fink, D. A. Walters, M. J. Casavant, J. Schmidt, and R. E. Smalley, *Synth. Met.* **121**, 1183 (2001).
  - [9] P. Longe and S. M. Bose, *Phys. Rev. B* **48**, 18239 (1993).
  - [10] C. S. Huang, M. F. Lin, and D. S. Chuu, *Solid State Commun.* **103**, 603 (1997).
  - [11] F. L. Shyu and M. F. Lin, *Phys. Rev. B* **62**, 8508 (2000).
  - [12] A. G. Marinopoulos, L. Reining, A. Rubio, and N. Vast, *Phys. Rev. Lett.* **91**, 046402 (2003).
  - [13] C. D. Spataru, S. Ismail-Beigi, L. X. Benedict, and S. G. Louie, *Phys. Rev. Lett.* **92**, 077402 (2004).
  - [14] E. Chang, G. Bussi, A. Ruini, and E. Molinari, *Phys. Rev. Lett.* **92**, 196401 (2004).
  - [15] A. G. Marinopoulos, L. Reining, V. Olevano, A. Rubio, T. Pichler, X. Liu, M. Knupfer, and J. Fink, *Phys. Rev. Lett.* **89**, 076402 (2002).
  - [16] A. G. Marinopoulos, L. Reining, A. Rubio, and V. Olevano, *Phys. Rev. B* **69**, 245419 (2004).
  - [17] J.-C. Charlier, X. Blase, and S. Roche, *Rev. of Mod. Phys.* **79**, 677 (2007).
  - [18] S. Baroni, P. Giannozzi, and A. Testa, *Phys. Rev. Lett.* **58**, 1861 (1987).
  - [19] F. Sottile, F. Bruneval, A. G. Marinopoulos, L. K. Dash, S. Botti, V. Olevano, N. Vast, A. Rubio, and L. Reining, *Int. J. Quantum Chem.* **102**, 684 (2005).
  - [20] Y. Murakami and S. Maruyama, *Chem. Phys. Lett.* **422**, 575 (2006).
  - [21] C. Kramberger, H. Shiozawa, H. Rauf, A. Grüneis, M. H. Rummeli, T. Pichler, B. Büchner, D. Batchelor, E. Einarsson, and S. Maruyama, *Phys. Stat. Solidi B* **244**, 3978 (2007).
  - [22] E. Einarsson, H. Shiozawa, C. Kramberger, M. H. Rummeli, A. Grüneis, T. Pichler, and S. Maruyama, *J. Phys. Chem. C* **111**, 17861 (2007).
  - [23] J. Fink, *Adv. Elec. & Elec. Phys.* **75**, 121 (1989).
  - [24] X. Gonze, J. M. Beuken, R. Caracas, F. Detraux, M. Fuchs, G. M. Rignanese, L. Sindic, M. Verstraete, G. Zerath, F. Jollet, et al., *Comp. Mat. Sci.* **25**, 478 (2002).
  - [25] N. Troullier and J. L. Martins, *Phys. Rev. B* **43**, 1993 (1991).
  - [26] M. Knupfer, T. Pichler, M. S. Golden, J. Fink, A. Rinzler, and R. E. Smalley, *Carbon* **37**, 733 (1999).